

Four-Point Bending Testing of 24-in. (600-mm) Diameter NS-type Ductile Iron Pipe

Shih-Hung Chiu

Shakhzod Takhirov

Kenichi Soga



Berkeley
CENTER FOR
Smart Infrastructure

CSI Report 2023/05
Center for Smart Infrastructure (CSI)
Department of Civil and Environmental Engineering
University of California, Berkeley July 2023

EXECUTIVE SUMMARY

In this report, the findings of an experiment conducted on a 24-inch NS-type ductile iron pipe manufactured by Kubota Corporation are reported. The main aim of this study is to evaluate the pipe's ability to withstand large bending deformation in the event of a geological hazard while maintaining its functionality over the expected service life. To assess the pipe's performance, a four-point bending test was conducted by applying a monotonic force perpendicular to the pipeline at the center of the specimens. The force applied gradually increased until the pipe sustained severe damage, leading to water leakage. Distributed fiber optic strain sensors were used to collect detailed information about the pipeline's behavior during the test. The data collected from these sensors provided a comprehensive understanding of the deformation and failure mechanisms observed during the experiment.

Keywords: *Ductil iron pipe, water pipelines, fiber optic, leakage, sensors.*

ACKNOWLEDGMENTS

The funding for this project was provided by the East Bay Municipal Utility District (EBMUD) and Kubota Corporation. The completion of the work would not be possible without the support of John Kochan, Irik Larson, and Phillip Wong of the University of California, Berkeley. Active involvement and guidance from David Katzev of EBMUD are greatly appreciated.

DISCLAIMER

Any opinions, findings, conclusions, or recommendations expressed in this material are those of the author(s) and do not necessarily reflect those of the University of California, Berkeley.

CONTENTS

EXECUTIVE SUMMARY	II
ACKNOWLEDGMENTS	III
DISCLAIMER	IV
CONTENTS	V
LIST OF FIGURES	VI
LIST OF TABLES	VII
1 Introduction	8
2 Experimental Setup	10
3 Instrumentation	11
3.1 Conventional Instruments	11
3.2 Fiber Optic Sensors	14
4 Test Results	16
4.1 Calculation Approach	16
4.2 Experimental Data Analysis	16
4.2.1 Moment and Rotation	16
4.2.2 Large Deformation and Failure Modes.....	18
4.2.3 Axial Strains	19
4.2.4 Hoop Strains	23
5 Conclusions	26
6 References	27
Appendix A: Distributed Fiber Optic Sensing	28
Appendix B: Fiber Optic Sensors Result	30

LIST OF FIGURES

Figure 1-1 Schematic of the bell of Kubota NS-type ductile iron pipe	9
Figure 1-2 Bell setup for the experiment	9
Figure 2-1 Experimental setup design	10
Figure 2-2 Overview of the experimental setup	11
Figure 3-1 Instrumentation plan of conventional instruments	12
Figure 3-2 DFOS instrumentation plan.....	15
Figure 4-1 Moment, rotation, and water pressure.....	17
Figure 4-2 Vertical wire pot measurements.....	17
Figure 4-3 Large deformation and failure.....	18
Figure 4-4 Failure of the gland and bolt	18
Figure 4-5 Failure of the spigot	19
Figure 4-6 Axial strain vs joint rotation.....	20
Figure 4-7 Axial strain development of bell pipe under 19-degree rotation condition. (a) East side, (b) Top side, (c) West side, (d) Bottom side	21
Figure 4-8 Axial strain development of spigot under 19-degree rotation condition. (a) East side, (b) Top side, (c) West side, (d) Bottom side	22
Figure 4-9 Hoop strain vs joint rotation.....	24
Figure 4-10 Strain distribution in the circumferential direction under 19-degree rotation condition. (a) sensor on the bell end (b) sensor on the center of the bell (c) sensor on the centerline of the specimen (d) sensor on the spigot.....	25

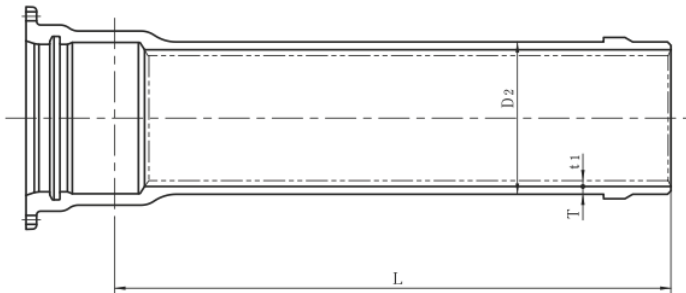
LIST OF TABLES

Table 3-1 Conventional instrumentation local names	12
Table 3-2 DFOS local names.....	15

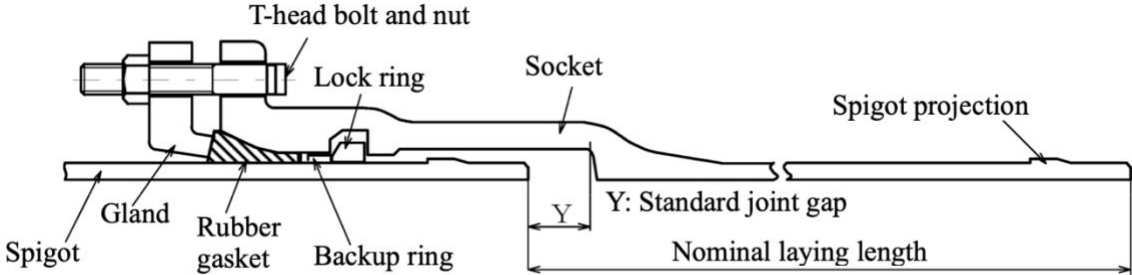
1 Introduction

This report provides a summary of the findings from a 4-point bending test conducted on a 24-inch Kubota NS-type ductile iron pipe. This pipe is designed to withstand seismic events and maintain full water service even in the aftermath of a ground failure. The joint connection of the pipe is built to withstand up to 2.4 inches of expansion and 10.2 inches of contraction. Additionally, it can accommodate a deflection angle of up to 7 degrees, which is important for adjusting to ground movement during a seismic event. The experiment aimed to determine the ultimate deflection capacity of the pipe, and the results will be valuable for ensuring its resilience in the face of geological hazards.

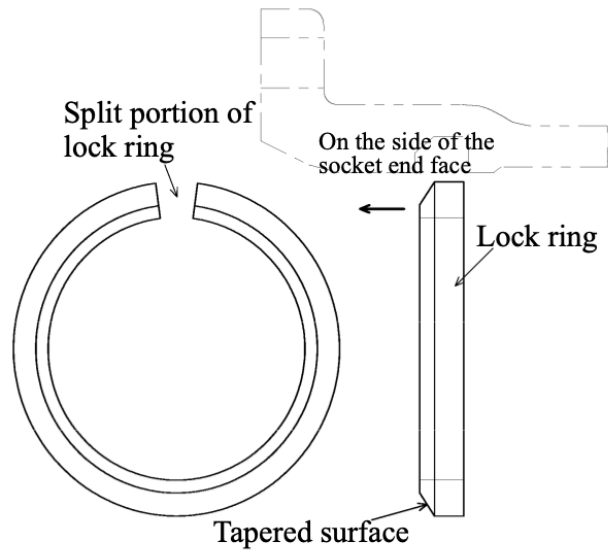
The pipe is equipped with a bell connection mechanism to join the two pipe sections together. The bell is a widened section at the end of each pipe section that facilitates the connection. The spigot, the tapered end of the pipe section, is designed to be inserted into the bell. Several components are employed in the assembly process to ensure a secure and watertight connection. First, a rubber gasket is utilized. The rubber gasket serves the purpose of preventing water leakage at the joint. It is positioned between the spigot and the bell, creating a seal when compressed. To hold the rubber gasket in place, a gland is used. The T-head bolt tightens the gland, which applies pressure to push the gland and secure the rubber gasket tightly. Next, a backup ring is incorporated into the joint assembly to provide additional support and protection to the rubber gasket. The backup ring is made of polyamide resin and acts as a buffer between the locking ring and the rubber gasket to prevent excessive stress on the rubber gasket. The locking ring, responsible for securely holding the joint, is designed with a split portion. This split portion allows for the installation of the locking ring into the socket groove of the bell. The split portion is positioned on the top during installation. The schematic of the bell is shown in Figure 1-1, whereas the assembled setup of the bell is shown in Figure 1-2.



(a) Cross section of the straight pipe (Kubota Co., 2020)



(b) Cross section of the bell (Kubota Co., 2014)



(c) Locking ring (Kubota Co., 2014)

Figure 1-1 Schematic of the bell of Kubota NS-type ductile iron pipe

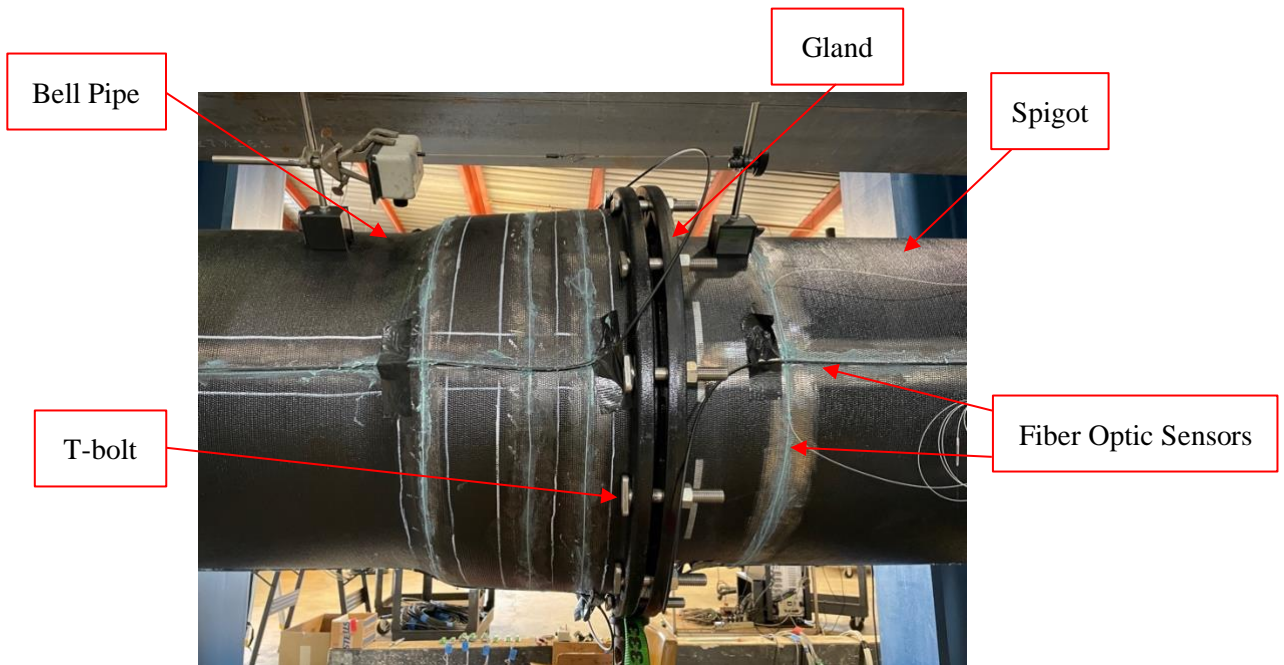


Figure 1-2 Bell setup for the experiment

Distributed fiber optic strain sensors (DFOS) were deployed to measure the continuous strain development along the longitudinal and circumferential directions. Conventional strain gauges were adopted for measuring strains at particular locations, and the results were compared to that acquired from DFOS. Wire pots were used for measuring the movement of the specimens. The failure mode and mechanism are discussed in the following sections using the experimental data.

2 Experimental Setup

The experimental setup used for the 4-point bending tests was developed at the Center for Smart Infrastructure (CSI) of UC Berkeley. The setup utilized hydraulic actuators and various support components to apply and transfer forces to the pipe specimens. Figure 2-1 and Figure 2-2 illustrate the setup. A 346-kip pulling and 462-kip pushing capacity with 36 inches total stroke hydraulic actuator was utilized in the experiments. The actuator was positioned at the center of the specimens, which was defined as 3.5 inches away from the bell. A steel spreader beam was placed beneath the actuator to facilitate load transfer. The force was initially applied to the beam and then transferred to two saddles on the pipes, located 72 inches from the center. The roller supports were situated 180 inches away from the center on both ends of the specimens.

The testing procedure includes three stages: water pressurization, self-weight moving down, and actuator pushing down. In the first stage, the pipes were pressurized with water up to a pressure of 70 psi. This pressurization simulated the internal pressure conditions that the pipeline would experience during their regular operation. In the second stage, the temporary supports initially in place were removed. This allowed the pipes to move downward under the influence of their self-weight. As the pipeline moved downward, small rotations were introduced into the specimens. Finally, the hydraulic actuator was employed in the third stage to push the pipeline further downward, inducing larger rotations in the specimen. The actuator applied a controlled force to the pipeline, progressively increasing the rotation until severe pipe damage and water leakage were observed. This stage aimed to test the ultimate deflection capacity of the pipe and assess its performance under severe bending forces.

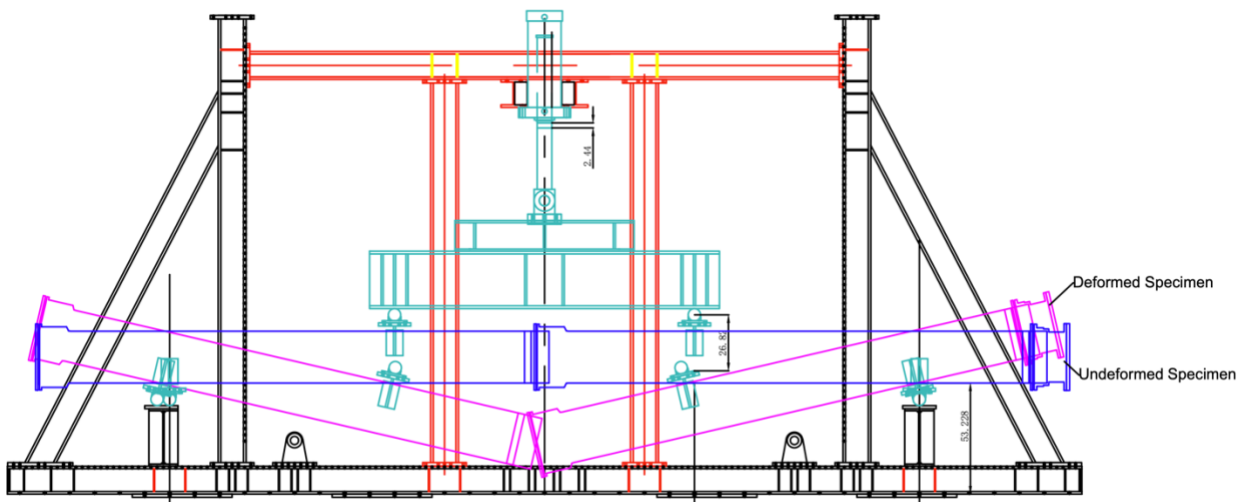


Figure 2-1 Experimental setup design



Figure 2-2 Overview of the experimental setup

3 Instrumentation

The instrumentation consisted of conventional instruments (strain gauges, wire pots, position transducer) and distributed fiber optic sensors (DFOS).

3.1 Conventional Instruments

The locations of the instruments are shown in Figure 3-1, and the local instrumentation names are given in Table 3-1.

In the experimental setup, conventional strain gauges were installed at four planes on the bell pipe and the spigot of the specimens. Each plane included four sets of strain gauges, resulting in a total of 32 strain gauges being installed. Each set of strain gauges comprised two strain gauges positioned in perpendicular directions to measure axial and circumferential strains. These strain gauges provided localized strain measurements along the pipe specimens at specific locations. Due to installation constraints and conflicts with the distributed fiber optic sensors (DFOS), the strain gauge sets were placed at approximately 9 degrees (2 inches) apart from the quarter points of the pipe specimens.

Eleven wire pots were installed on the specimens to measure the displacements. Four wire pots were used to measure the joint opening, located 45 degrees apart from the quarter points. Seven additional wire pots were placed beneath the specimen to monitor vertical displacements of the pipes. The exact locations of the instruments are shown in Figure 3-1 and Figure 3-2. The local instrument names are shown in Table 3-1.

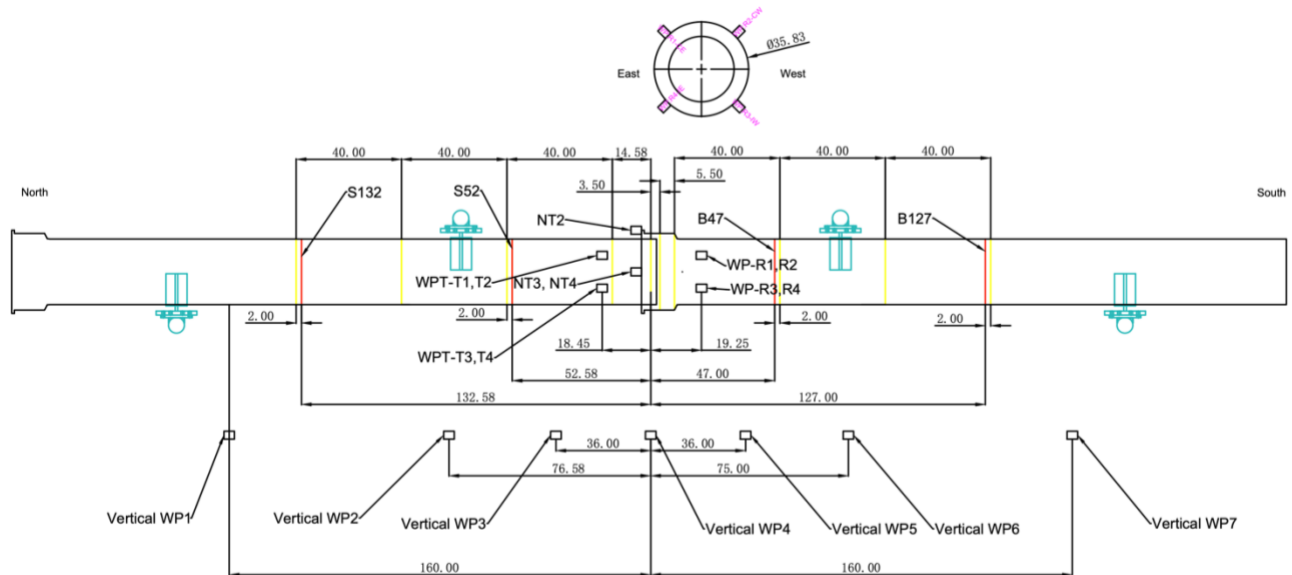


Figure 3-1 Instrumentation plan of conventional instruments

Table 3-1 Conventional instrumentation local names

Instrument	Location	Instrument Description	Position	Instrument Designation
Strain Gauge	-132.5 in. from Centerline	Axial Gage at Crown on Spigot End	Radial	S132C-R
	-132.5 in. from Centerline	Axial Gage at Crown on Spigot End	Longitudinal	S132C-L
	-132.5 in. from Centerline	Axial Gage at West on Spigot End	Radial	S132W-R
	-132.5 in. from Centerline	Axial Gage at West on Spigot End	Longitudinal	S132W-L
	-132.5 in. from Centerline	Axial Gage at Invert on Spigot End	Radial	S132I-R
	-132.5 in. from Centerline	Axial Gage at Invert on Spigot End	Longitudinal	S132I-L
	-132.5 in. from Centerline	Axial Gage at East on Spigot End	Radial	S132E-R
	-132.5 in. from Centerline	Axial Gage at East on Spigot End	Longitudinal	S132E-L
	-52.5 in. from Centerline	Axial Gage at Crown on Spigot End	Radial	S52C-R
	-52.5 in. from Centerline	Axial Gage at Crown on Spigot End	Longitudinal	S52C-L
	-52.5 in. from Centerline	Axial Gage at West on Spigot End	Radial	S52W-R
	-52.5 in. from Centerline	Axial Gage at West on Spigot End	Longitudinal	S52W-L
	-52.5 in. from Centerline	Axial Gage at Invert on Spigot End	Radial	S52I-R

	-52.5 in. from Centerline	Axial Gage at Invert on Spigot End	Longitudinal	S52I-L
	-52.5 in. from Centerline	Axial Gage at East on Spigot End	Radial	S52E-R
	-52.5 in. from Centerline	Axial Gage at East on Spigot End	Longitudinal	S52E-L
	47 in. from Centerline	Axial Gage at Crown on Bell End	Radial	B47C-R
	47 in. from Centerline	Axial Gage at Crown on Bell End	Longitudinal	B47C-L
	47 in. from Centerline	Axial Gage at West on Bell End	Radial	B47W-R
	47 in. from Centerline	Axial Gage at West on Bell End	Longitudinal	B47W-L
	47 in. from Centerline	Axial Gage at Invert on Bell End	Radial	B47I-R
	47 in. from Centerline	Axial Gage at Invert on Bell End	Longitudinal	B47I-L
	47 in. from Centerline	Axial Gage at East on Bell End	Radial	B47E-R
	47 in. from Centerline	Axial Gage at East on Bell End	Longitudinal	B47E-L
	127 in. from Centerline	Axial Gage at Crown on Bell End	Radial	B127C-R
	127 in. from Centerline	Axial Gage at Crown on Bell End	Longitudinal	B127C-L
	127 in. from Centerline	Axial Gage at West on Bell End	Radial	B127W-R
	127 in. from Centerline	Axial Gage at West on Bell End	Longitudinal	B127W-L
	127 in. from Centerline	Axial Gage at Invert on Bell End	Radial	B127I-R
	127 in. from Centerline	Axial Gage at Invert on Bell End	Longitudinal	B127I-L
	127 in. from Centerline	Axial Gage at East on Bell End	Radial	B127E-R
	127 in. from Centerline	Axial Gage at East on Bell End	Longitudinal	B127E-L
Wire Pot	160 in. from Centerline	WP Position transducer on Spigot End	Vertical	WP1-S160
	76.5 in. from Centerline	WP Position transducer on Spigot End	Vertical	WP2-S76
	36 in. from Centerline	WP Position transducer on Spigot End	Vertical	WP3-S36
	0 in. from Centerline	WP Position transducer on Bell End	Vertical	WP4-B0
	36 in. from	WP Position transducer on	Vertical	WP5-B36

	Centerline	Bell End		
	75 in. from Centerline	WP Position transducer on Bell End	Vertical	WP6-B75
	160 in. from Centerline	WP Position transducer on Bell End	Vertical	WP7-B160
	38 in. between WPs and WP Targets	WP Position transducer at Crown-East on Bell End	Bell to Spigot 45-Degree	WPR1-CE
	38 in. between WPs and WP Targets	WP Position transducer at Crown-West on Bell End	Bell to Spigot 45-Degree	WPR2-CW
	38 in. between WPs and WP Targets	WP Position transducer at Invert-West on Bell End	Bell to Spigot 45-Degree	WPR3-IW
	38 in. between WPs and WP Targets	WP Position transducer at Invert-East on Bell End	Bell to Spigot 45-Degree	WPR4-IE
Position Transducer	Gland to Flange	Novotechnik Position transducer at Top on Joint		NT2-C
	Gland to Flange	Novotechnik Position transducer at West on Joint		NT3-W
	Gland to Flange	Novotechnik Position transducer at East on Joint		NT4-E

3.2 Fiber Optic Sensors

Two types of fiber optic cables manufactured by NanZee Sensing Technology Co. were utilized to capture strain measurements: (a) 5 mm diameter armored cable (NanZee 5mm) and (b) 0.9 mm diameter cable (NanZee 0.9mm). To attach the fiber optic cables to the pipes, 3M SCOTCH-WELD DP8010 epoxy was used. Figure 3-2 illustrates the layout and locations of the sensors. The NanZee 5mm cables, represented by blue lines, were employed in the longitudinal direction of the pipes to mimic real-world construction site applications. They were attached to both pipes at locations 90 degrees apart, numbered F11 to F18. These sensors captured longitudinal strains along the pipes. On the other hand, the NanZee 0.9mm cables, represented by red lines, numbered F1-F10, were used to measure circumferential strains and gain a better understanding of the deformation mechanism of the pipes. Seven circumferential sensors with about 40-inch spacing were installed on the pipes. In addition, another three circumferential sensors were attached to the bell (bell end, middle of the bell, and at the centerline of the specimen). The local names of DFOS are listed in Table 3-2.

A Rayleigh-based optical frequency domain reflectometry (OFDR), Luna ODiSI 6100 series, was used in the experiments for data acquisition. The analyzer is capable of measuring up to 50m long fiber optic cable with an accuracy of less than ± 1 micro strain when taking a measurement every 0.65mm. Appendix A provides more information about the cables and the analyzer.

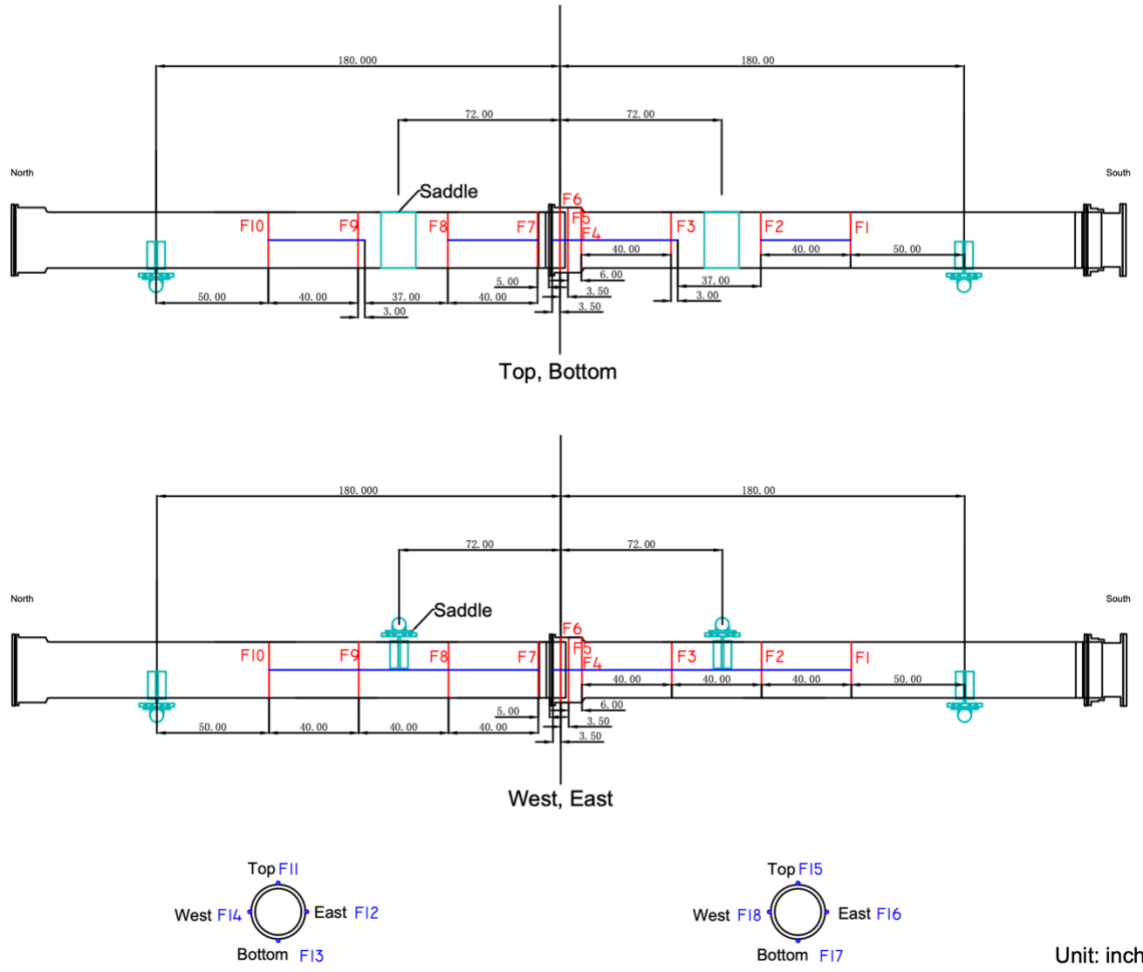


Figure 3-2 DFOS instrumentation plan

Table 3-2 DFOS local names

Instrument	Location	Local Instrument Name
DFOS	129.5 inch south of centerline, Circumferential	F1
	89.5 inch south of centerline, Circumferential	F2
	49.5 inch south of centerline, Circumferential	F3
	9.5 inch south of centerline, Circumferential	F4
	3.5 inch south of centerline, Circumferential	F5
	On the centerline, Circumferential	F6
	8.5 inch north of center, Circumferential	F7
	48.5 inch north of center, Circumferential	F8
	88.5 inch north of center, Circumferential	F9
	128.5 inch north of center, Circumferential	F10
	Spigot, Top, Longitudinal	F11
	Spigot, East, Longitudinal	F12
	Spigot, Bottom, Longitudinal	F13
	Spigot, West, Longitudinal	F14
	Bell pipe, Top, Longitudinal	F15
	Bell pipe, East, Longitudinal	F16

	Bell pipe, Bottom, Longitudinal	F17
	Bell pipe, West, Longitudinal	F18

4 Test Results

All test results are discussed in this section. In addition, a summary of the failure mode and performance of the 24 inch Kubota NS-type ductile iron pipe is included.

4.1 Calculation Approach

The approaches to calculating the rotation and moment are discussed herein. The pipes are assumed to be rigid bodies, and the rotations of the pipes are computed using equations (1) – (3). The vertical displacements of the pipes were measured by the vertical wire pots (VWP) that are the closest to the end supports (i.e., wp1 and wp7). θ_{bell} and θ_{spigot} are the rotations of the bell pipe and the spigot, respectively. The overall rotation, θ_{Total} , of the joint is defined as the sum of the two side angles. The distance between the VWP and the end support for both pipes is 20 inches.

$$\theta_{bell} = \tan^{-1}\left(\frac{\text{vertical displacement of bell pipe}}{\text{distance between VWP and the end support}}\right) \quad (1)$$

$$\theta_{spigot} = \tan^{-1}\left(\frac{\text{vertical displacement of spigot}}{\text{distance between VWP and the end support}}\right) \quad (2)$$

$$\theta_{Total} = \theta_{bell} + \theta_{spigot} \quad (3)$$

The system is considered to be a simple-supported beam. The self-weight, including the weights of the pipe and water, is assumed to be evenly distributed, and hence the moment introduced by self-weight is calculated based on equation (4), where w is the uniform load due to the self-weight, and l is the length of the pipe between the supports. The uniform weight (w) is 24.9 lbs/in and the distance between the supports (l) is 360 inches. The additional moment applied to the central portion of the pipe is calculated using equation (5), where P is the actuator load, and L is the distance between the support and the loading location (i.e., 108 inches).

$$M_{distrib} = \frac{wl^2}{8} \quad (4)$$

$$M_{central} = \frac{PL}{2} \quad (5)$$

4.2 Experimental Data Analysis

4.2.1 Moment and Rotation

During the experimental testing, the pipes were filled with water and pressurized to a level of 70 psi. A monotonic force, perpendicular to the longitudinal axis of the pipeline, was applied at

the center point of the load transfer beam. This force was then transferred to the pipes through the two loading saddles. Using the formulas specified in the previous section, the moments and rotations of the specimen were calculated. The results are visualized in Figure 4-1. The maximum rotation is about 20 degrees. This rotation is approximately three times larger than the manufacturer's specified deflection capacity, which is mentioned to be 7 degrees. The maximum moment is about 3,313 kip-in. In addition, no water leakage was detected in the specimens until the pipe joint reached a rotation of approximately 20 degrees.

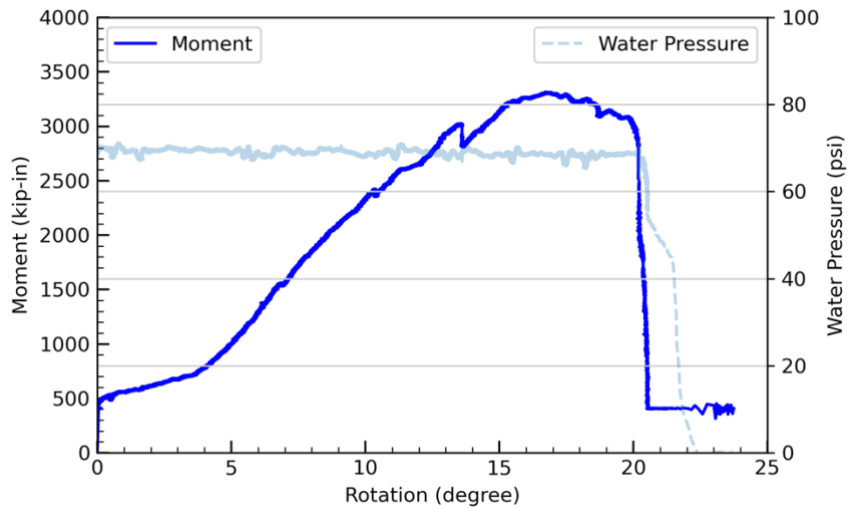


Figure 4-1 Moment, rotation, and water pressure

Figure 4-2 displays the vertical wire pot (VWP) measurements obtained at different distances from the center point during the experimental testing. The VWP measurements taken on both the spigot side and bell side show a good agreement in terms of vertical movement, meaning that at equal distances from the center point of the specimen, the vertical displacements measured on the spigot side and bell side of the pipes align closely. This indicates that the pipe exhibits symmetric behavior under the applied bending forces.

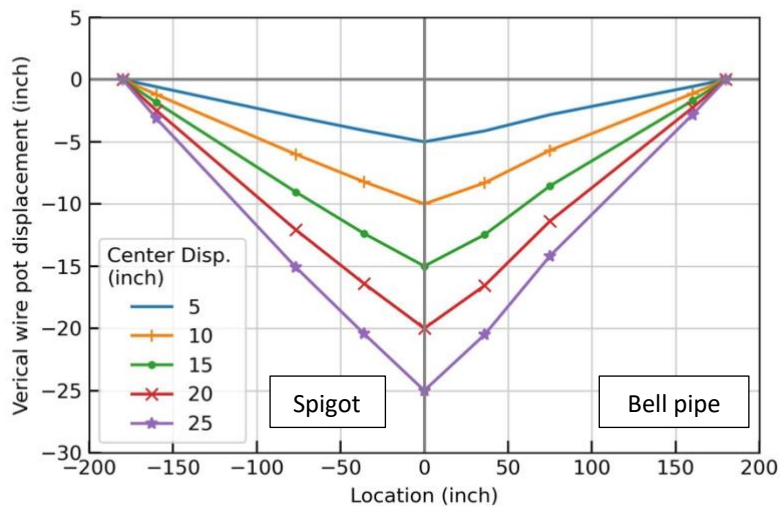


Figure 4-2 Vertical wire pot measurements

4.2.2 Large Deformation and Failure Modes

Figure 4-3 shows the figure of the specimen with large deformation and failure. Notably, a large crack was observed on the spigot while the specimen reached about 20-degree deflection, followed by significant water leakage. On the other hand, no apparent failure was observed on the bell section of the specimen. In addition, Figure 4-4 illustrates a portion of the gland that experienced failure on the top side, where the bolts were bent. This failure occurred due to the interaction between the gland and the spigot during the downward pushing of the pipe. As the gland exerted pressure against the spigot, a large shearing force was generated, leading to the cutting of the gland material. Consequently, this introduced significant deformation to the surrounding bolts, resulting in their bending.

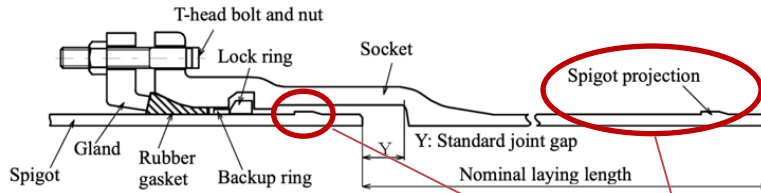


Figure 4-3 Large deformation and failure



Figure 4-4 Failure of the gland and bolt

The cracks observed on the spigot of the specimen originated from the edge of the spigot projection, located approximately 2-¼ inches from the spigot end, as shown in Figure 4-5. During the pushing-down process, the top side of the spigot exhibited a tendency to move inward towards the bell, while the bottom side tended to move away from the bell. Consequently, the bottom side of the spigot projection made full contact with the locking ring, resulting in a brittle tensile failure at the bottom side of the edge of the spigot projection. This specific location experienced a high stress concentration due to the contact forces and interactions between the spigot and the locking ring.



(a) West side



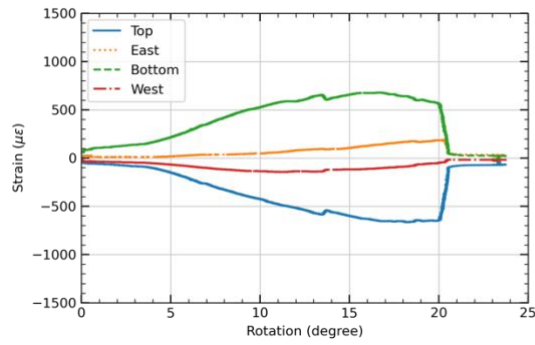
(b) East side

Figure 4-5 Failure of the spigot

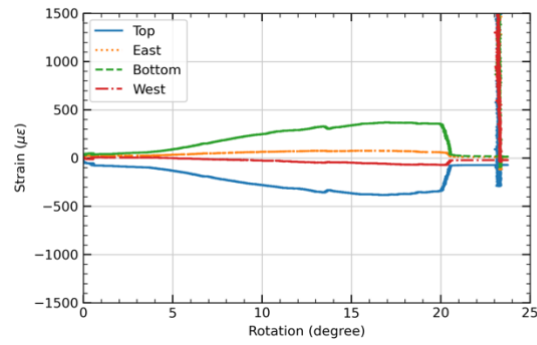
The initial crack at the edge of the bottom of the spigot projection then proceeded to propagate through the sides towards the top side. Shear forces primarily drove this propagation. The combination of the stress concentration at the edge of the spigot projection and the shear forces resulted in the formation and progression of the observed cracks, ultimately leading to the failure of the spigot and the subsequent water leakage.

4.2.3 Axial Strains

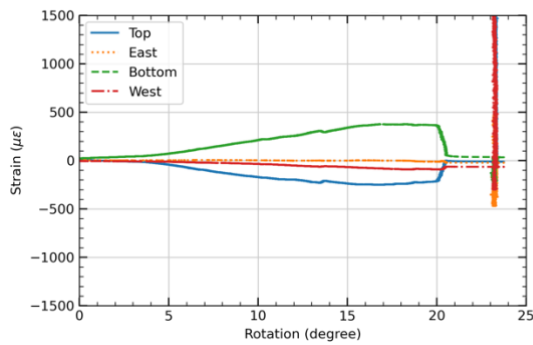
The axial strain results measured by the conventional strain gauges attached to the specimen are shown in Figure 4-6. Generally, the top side of the pipe (12 o'clock position) experiences compression. In comparison, the bottom side (6 o'clock position) undergoes tension. Theoretically, the axial strains at the east side (9 o'clock) and west side (3 o'clock) would be close to zero. However, due to installation constraints, the strain gauges were attached with a 9-degree (i.e., 2 inches) offset from the quarter points. As a result, the strain gauges labeled "east" were positioned 9 degrees towards the bottom side (6 o'clock), causing them to measure tension. Conversely, the strain gauges labeled "west" were located 9 degrees towards the top side (12 o'clock), leading to compression measurements.



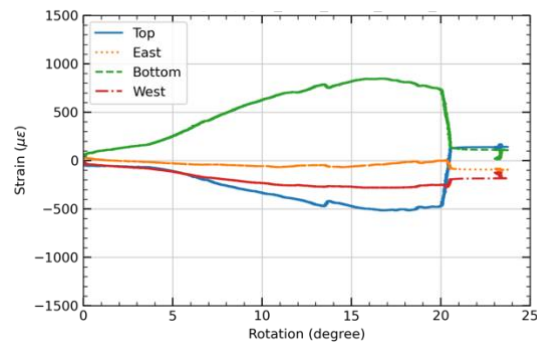
(a) Bell Pipe (North)



(b) Bell Pipe (South)



(c) Spigot (North)



(d) Spigot (South)

Figure 4-6 Axial strain vs joint rotation

The axial strain results measured by DFOS are shown in Figure 4-7 and Figure 4-8. The strain gauge data are also plotted to show the two data sets are compatible with each other. The plots show the strain distribution when the total rotation reached about 19 degrees. All the strain distributions of the sensors are plotted from the north to the south. Consistent with the observations made from the strain gauge data, the plots illustrate that the top side of the pipe (12 o'clock) was subjected to compression, while the bottom side (6 o'clock) experienced tension. Additionally, the strains measured at the sides of the pipe (i.e., 3 o'clock and 9 o'clock) were generally minimal. This observation aligns with the pipe's theoretical expectation under bending forces.

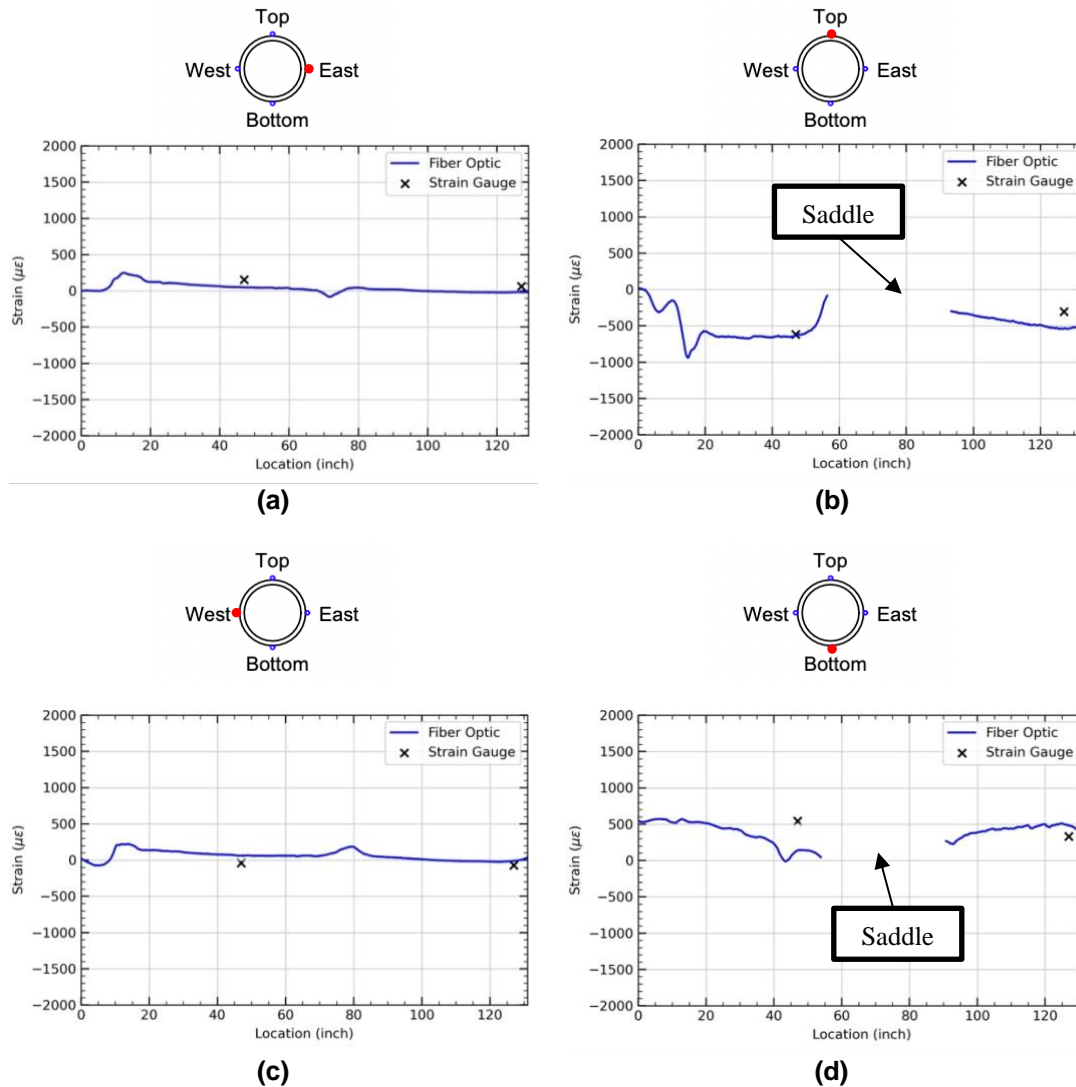


Figure 4-7 Axial strain development of bell pipe under 19-degree rotation condition. (a) East side, (b) Top side, (c) West side, (d) Bottom side

Figure 4-7 shows the axial strain results of the bell pipe. Compressive strains were observed on both the west and east sides (3 o'clock and 9 o'clock positions) of the bell section (i.e., about 0 to 10 inches location), as depicted in Figure 4-7 (a) and (c). This compressive strain pattern can be attributed to the expansion of the bell caused by the locking ring. As the bell expands, a moment is introduced on its surface, leading to compressive strains on the bell's outer surface. On the top side, as shown in Figure 4-7 (b), relatively small compressive strains were observed on the bell section. This might be because the split of the locking ring was located on the top side. While the pipe is being pushed downward, the locking ring might deformed or moved upward in order to tolerate the movement, which might result in tensile stress at the bell section.

Following the bell section (i.e, about 10 to 20 inches location), large tensile strains can be observed on the west and east side of the bell pipe, as shown in Figure 4-7 (a) and (c), and large compressive strains on the top side of the bell pipe, as shown in Figure 4-7 (b). These locations correspond to the transition location from the bell to the pipeline. This phenomenon can be attributed to the geometry and wall thickness changes at this transition region. The altered geometry and wall thickness can lead to localized stress concentrations, resulting in the observed

strain patterns. The exact causes and mechanisms behind these strain variations will be further investigated through future finite element (FE) analysis.

Examining Figure 4-7 (a) and (c) in the axial strain results, noticeable strain fluctuations were observed at the loading saddle locations, which are situated at approximately 70-80 inches locations. These fluctuations were raised due to the concentrated forces acting within these regions during the bending tests. As a result, the pipe experiences larger deformation in these specific areas, leading to larger strains.

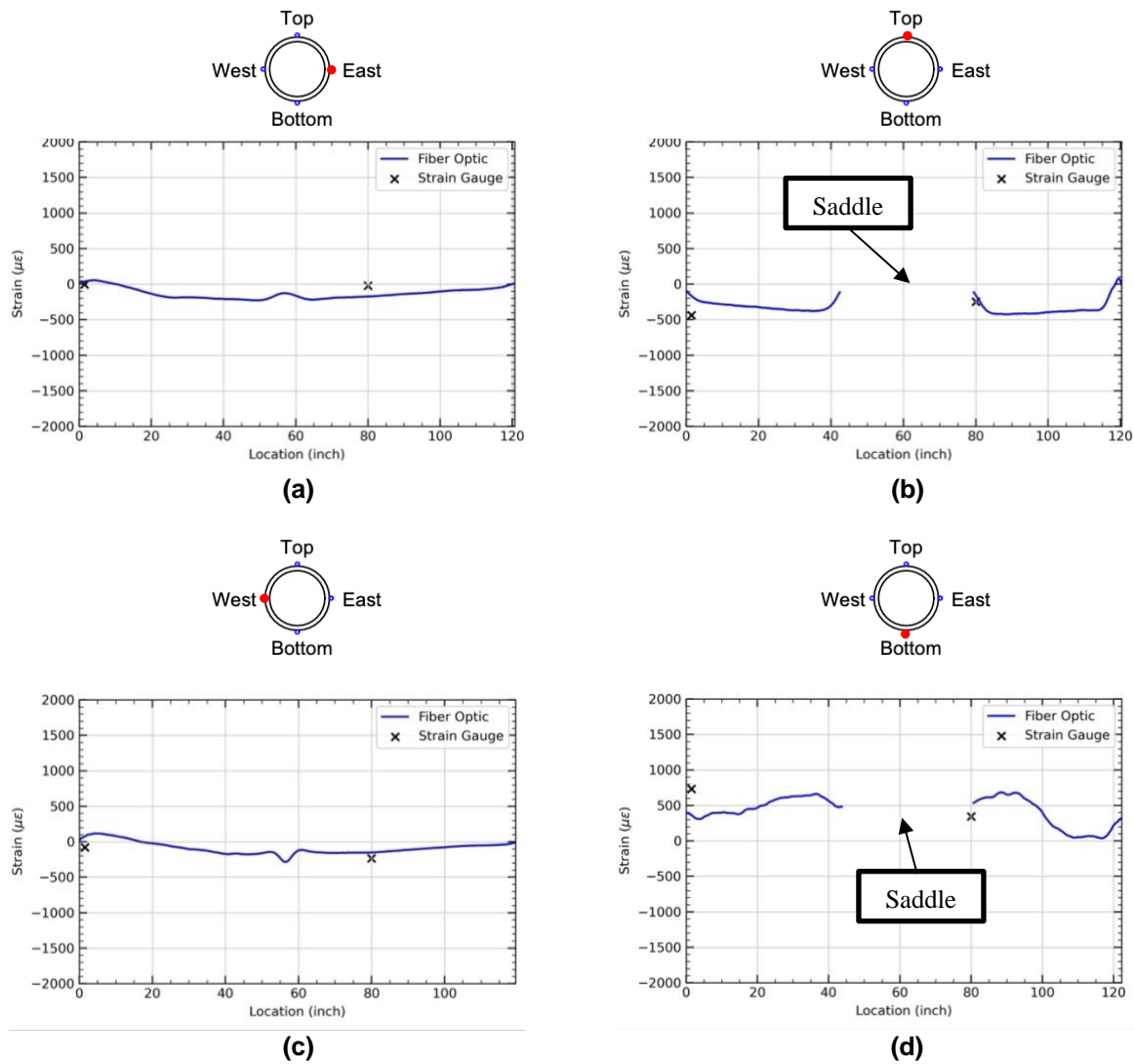


Figure 4-8 Axial strain development of spigot under 19-degree rotation condition. (a) East side, (b) Top side, (c) West side, (d) Bottom side

Figure 4-8 presents the axial strain results of the spigot under conditions where the rotation reaches approximately 19 degrees, which is close to the failure stage. The observed strain patterns align with the bending theorem, with compressive strains on the top side (12 o'clock) and tensile strains on the bottom side (6 o'clock) of the spigot. Additionally, minimal strains are recorded on the west and east sides (3 o'clock and 9 o'clock), as expected.

However, it is noteworthy that relatively smaller tensile strains were observed at the bottom side of the spigot near the bell, specifically in the 100-120 inches location shown in Figure 4-8 (d). This phenomenon might be attributed to the yielding or cracking at the bottom side of the spigot prior to failure (when the specimen reached approximately 20 degrees of rotation). The existence of these potential yielding/ cracking areas affected the proper transfer of stress at these particular locations, resulting in smaller tensile strains being measured.

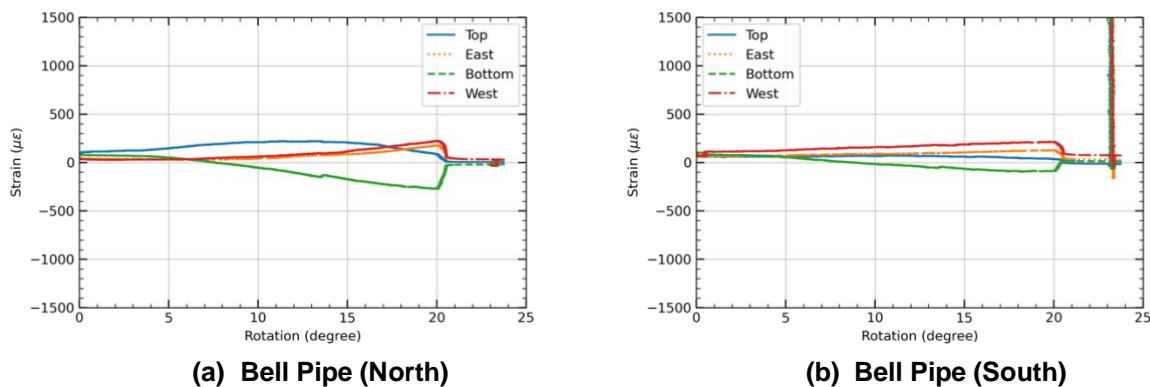
Furthermore, a significant deformation was observed on the spigot near the bell. This deformation and the Poisson's ratio effect may contribute to the small tensile strains measured in this region. The axial deformation and associated stress concentration near the bell might lead to a reduction in tensile strains. The presence of yielding/ cracking areas and the Poisson's effect are potential factors influencing the observed strain behavior in the spigot near the bell. These issue will be carefully discussed in the finite element analysis planned in the future.

Lastly, a fluctuation of the strains near the loading saddle, approximately 50-60 inches locations, was observed on the west and east sides of the spigot, as shown in Figure 4-8 (a) and (c). These strain fluctuations can be attributed to the concentrated forces applied at these locations. The concentrated force application created a localized stress concentration, resulting in large deformation of the pipe in that region. As a consequence, larger strain values were recorded.

4.2.4 Hoop Strains

Figure 4-9 displays the relationships between the hoop strains, measured by strain gauges, and the rotation of the pipe specimen. Initially, when the specimen rotation is small (less than 3 degrees), the strains in the circumferential direction are primarily opposite in direction to those in the longitudinal direction, but with a smaller magnitude. This behavior can be attributed to the Poisson's effect, which refers to the lateral expansion or contraction of a material due to axial deformation.

However, as the rotation increases beyond this small range, the strain results exhibit a different pattern. The bell pipe and the spigot demonstrate expansion at the east and west sides, while experiencing shrinkage at the top and bottom sides. This distinctive strain pattern indicates that the pipe undergoes a squatting deformation. A clear mechanism of the pipe deformation is provided in the following section using the DFOS data.



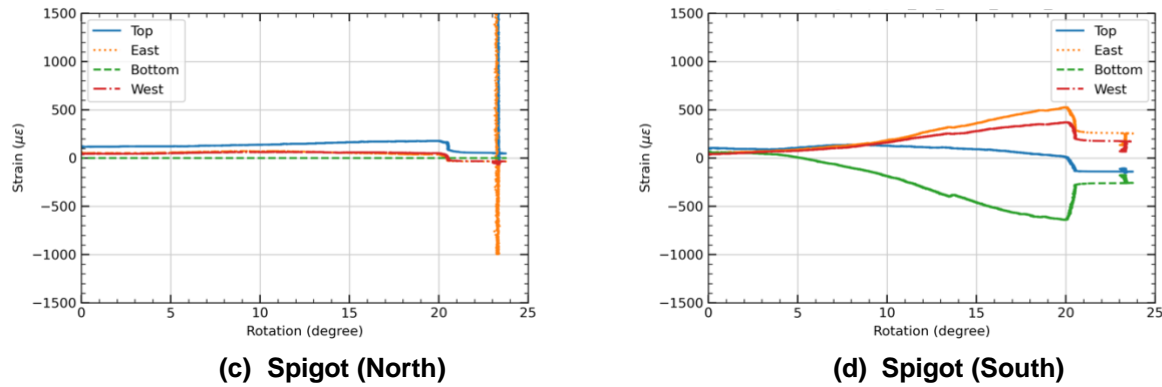


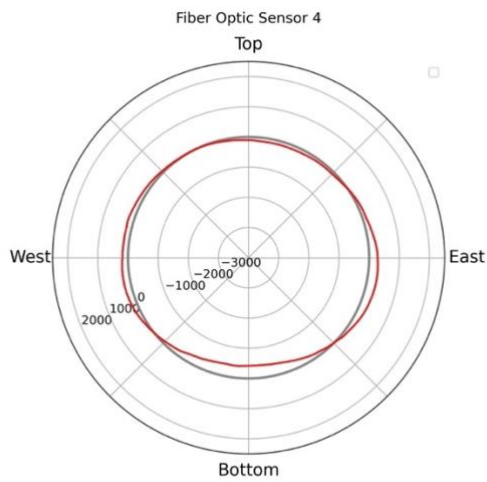
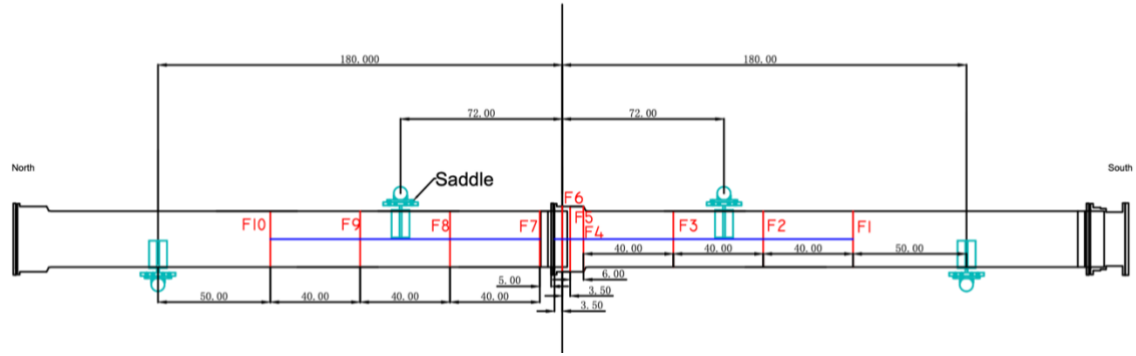
Figure 4-9 Hoop strain vs joint rotation

In Figure 4-10, the hoop strain results measured by DFOS are presented. The figures include the results obtained from sensor F4, which was placed on the bell end, sensor F5 located in the middle of the bell, sensor F6 positioned on the centerline, and sensor F7 on the spigot, which is the circumferential sensor closest to the bell. Additional hoop strain results for other sensors can be found in Appendix B.

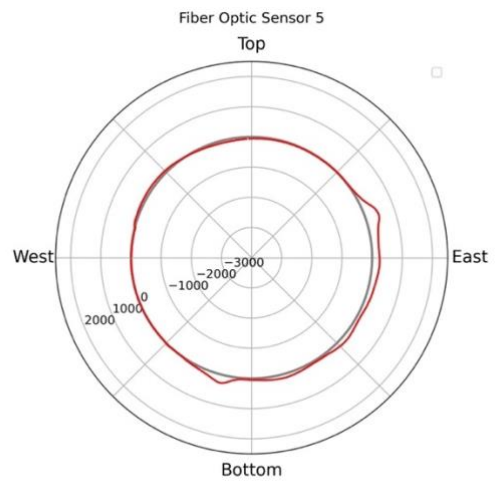
The results from sensor F4 indicate that the top and bottom sides (12 o'clock and 6 o'clock) of the bell were experiencing compression, while the west and east sides (3 o'clock and 9 o'clock) were expanding. These strain distributions suggest that the bell pipes undergo eccentric squatting during bending. Similar strain patterns can be observed on the other circumferential sensors located on the bell pipes (i.e., F1-F3).

For sensors F5 and F6, the results indicate that the bottom side of the bell was expanding. This expansion is attributed to the contact between the bottom of the spigot and the invert of the bell during bending. This contact causes the bottom side of the bell to expand.

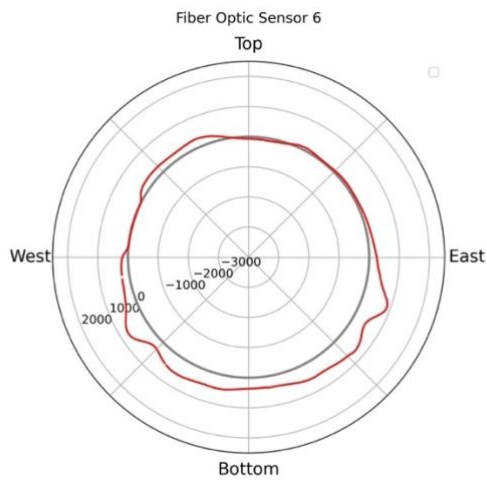
Sensor F7, placed on the spigot, exhibits a strain distribution where the top and bottom sides (12 o'clock and 6 o'clock) are shrinking, while the east and west sides (3 o'clock and 9 o'clock) are expanding. This behavior is attributed to the bottom side of the spigot bearing against the invert of the bell, leading to compression on the bottom side. Furthermore, as the spigot is bent, the top side contacts the crown of the bell, resulting in a concentrated compressive strain on the top of the spigot. Similar strain patterns can be observed from other sensors placed on the spigot (i.e., F8-F10), with the magnitude of the strain decreasing as the distance from the sensor to the bell increases.



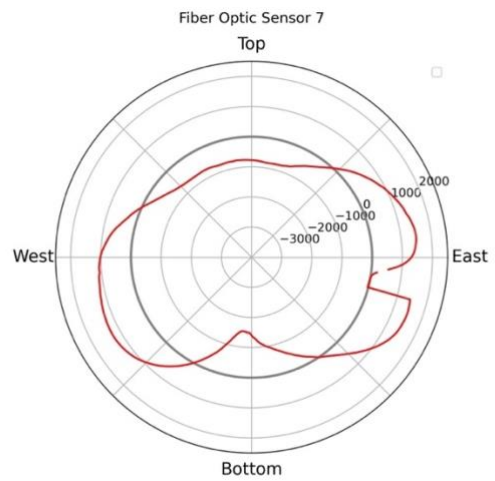
(a)



(b)



(c)



(d)

Figure 4-10 Strain distribution in the circumferential direction under 19-degree rotation condition. (a) sensor on the bell end (b) sensor on the center of the bell (c) sensor on the centerline of the specimen (d) sensor on the spigot

5 Conclusions

The 4-point bending test carried out on a 24-inch Kubota NS-type ductile iron pipe exhibited noteworthy results. The pipe surpassed the manufacturer's deflection capacity as it was able to achieve a maximum rotation of about 20 degrees. During this rotation, a tensile crack was noticed at the bottom of the spigot projection, which then propagated through the sides to the top side due to the shear forces, ultimately resulting in the spigot's failure. It is worth noting that there was no water leakage detected before the pipe reached the 20-degree rotation. The maximum moment observed during the test was around 3,313 kip-in.

Strain measurements obtained from distributed fiber optic sensors (DFOS) and strain gauges provided valuable insights into the behavior of the pipe. The strain distribution indicated that the pipe experienced compression on the top and bottom sides and expansion on the east and west sides. At the bell section, additional expansion on the bottom side was found due to the interaction between the bell and the spigot. The vertical displacements measured by the vertical wire pots on both the spigot and bell pipe demonstrated close alignment, suggesting symmetric behavior under the applied bending forces.

These findings provide valuable insights into the pipe's ultimate deflection capacity, failure mechanisms, and deformation behavior when subjected to bending forces. The strain measurements gathered from both DFOS and strain gauges are crucial in developing and validating numerical models for future analyses and simulations. With this information, we can better understand how pipes behave under different conditions and make more accurate predictions about their performance.

6 References

Kubota Co. (2020). Dimension Handbook [Brochure].

https://www.kubota.com/products/ironpipe/tech_info/pdf/Dimension_handbook/NS-Type_DimensionHandbook.pdf

Kubota Co. (2014). Assembling Procedure of 20"-40" NS Joint [Brochure].

https://www.kubota.com/products/ironpipe/tech_info/pdf/Assembling_manual/NS-Type_Joint.pdf

Wu, J., Jiang, H., Su, J., Shi, B., Jiang, Y., & Gu, K. (2015). Application of distributed fiber optic sensing technique in land subsidence monitoring. *Journal of Civil Structural Health Monitoring*, 5(5), 587-597.

Appendix A: Distributed Fiber Optic Sensing

Using the physical properties of light, fiber-optic sensing can detect changes in temperature, strain, and other parameters when light travels along a fiber, which uses fiber-optic cables as sensors and can measure over long distances at 100 to 1000s of points on a single cable or multiplexed cables depending on the analyzer used. Compared to the other sensing technologies, fiber-optic sensing has distinct advantages such as small size, light weight, and strong resistance to corrosion and water. Distributed fiber optic sensing consists of two main components, an analyzer, and fiber-optic cables. LUNA ODiSI 6000 series interrogator was used as the analyzer, and NanZee Sensing Technology Co manufactured the fiber-optic cables in the experiments.

LUNA Interrogator




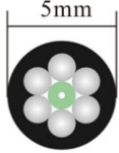
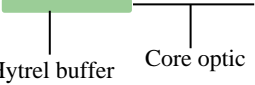
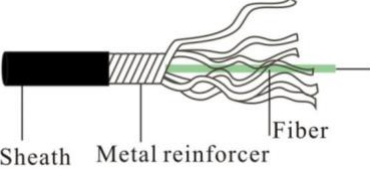
Figure A-1. LUNA ODiSI 6000 Series optical distributed sensor interrogator (LUNA, 2022)

LUNA ODiSI 6104 is an optical distributed sensor interrogator that can provide thousands of strain or temperature measurements per meter of a single high-definition fiber sensor. High-Definition H.D.D) Sensors - Strain & Temperature (HD-SC) temperature sensors utilize an advanced interrogation mode of the ODiSI to increase the accuracy of measurements when the sensors are subjected to strain, such as in embedded and surface-mount installations. It can achieve a sensor gauge pitch (the distance between two measurement points) as small as 0.65 mm, a sensor length of up to 50 m, and a measurement rate of up to 250 Hz with an accuracy of less than ± 1 microstrain.

Fiber-optic Cable

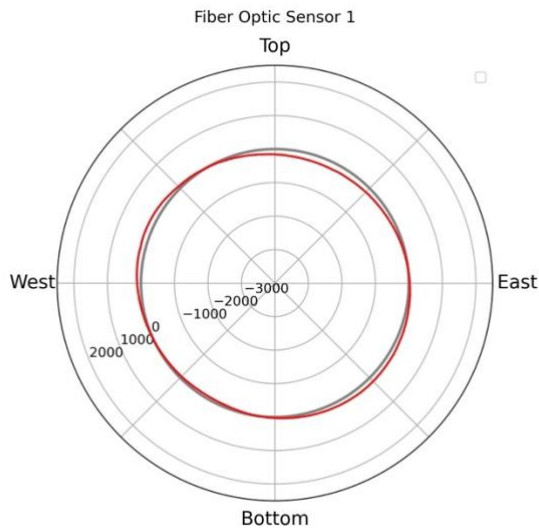
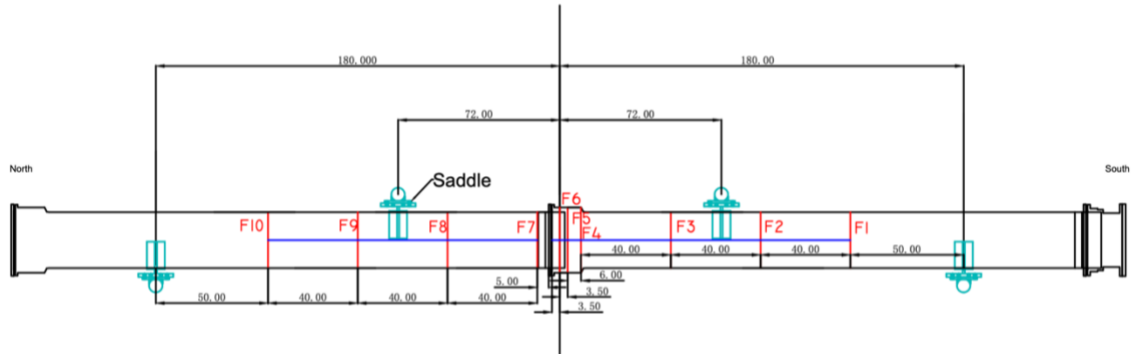
Two types of fiber optic cables manufactured by NanZee Sensing Technology Co. were used; (a) 5 mm diameter armored cable (NanZee 5mm) and (b) 0.9 mm diameter cable (NanZee 0.9mm). Table A-1 lists the information on the cables. The difference between the two cables is the thickness and material of the coating. NanZee, a 5mm cable, provides a sheath layer and steel reinforcement, resulting in better protection to the optical core; hence, it can be used for the actual field application. The coating of NanZee 0.9mm cable is thinner than NanZee 5mm cable. NanZee 0.9mm cable has less protection, but a more sensitive strain response is achieved.

Table A-1 Schematic illustration of the selected strain sensor cable (Wu et al., 2015)

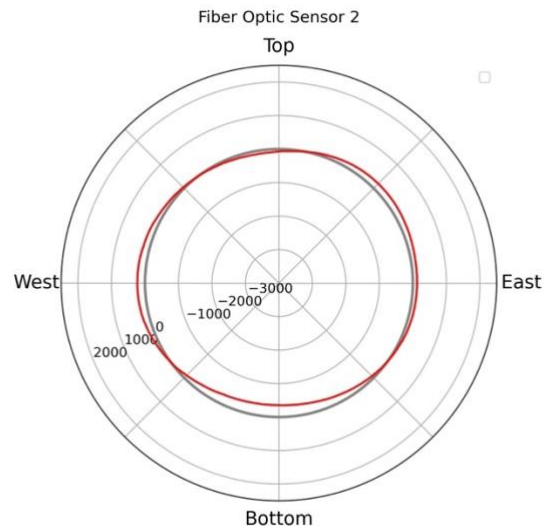
Brand	NanZee Sensing Technology Co.	
Model	NZS-DSS-C07	NZS-DSS-C02
Cross section	 <p>0.9mm</p>	 <p>5mm</p>
Side view	 <p>Hytel buffer Core optic</p>	 <p>Sheath Metal reinforcer Fiber</p>

Appendix B: Fiber Optic Sensors Result

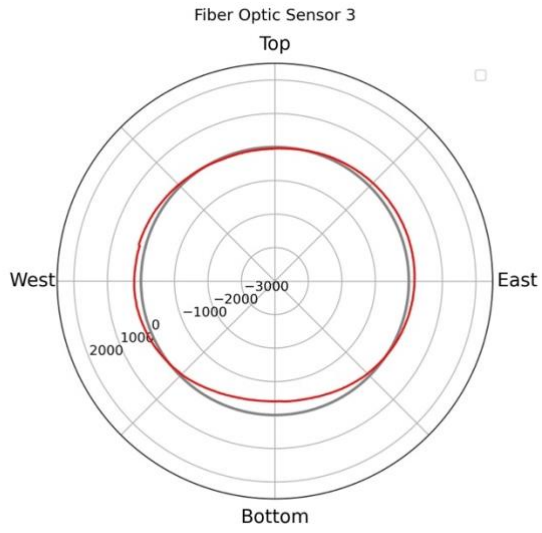
The hoop strain results from the distributed fiber optic sensors are demonstrated herein.



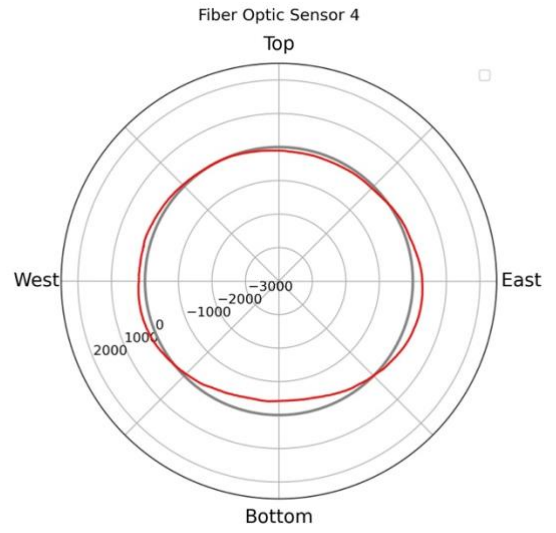
(a) Fiber Optic Sensor F1



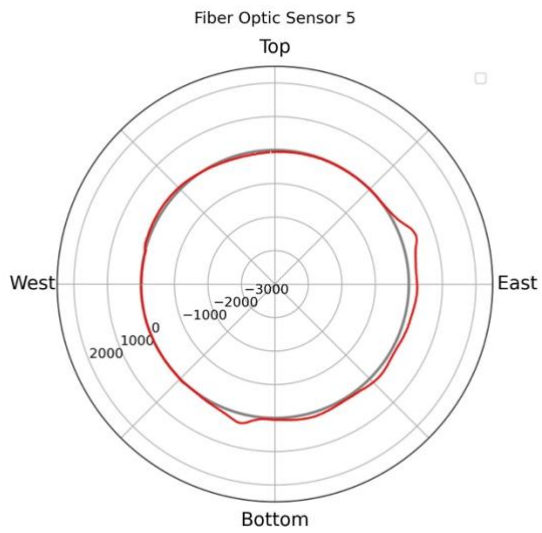
(b) Fiber Optic Sensor F2



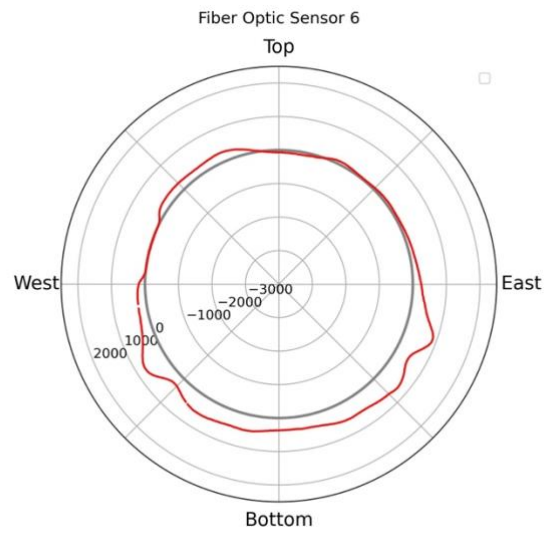
(c) Fiber Optic Sensor F3



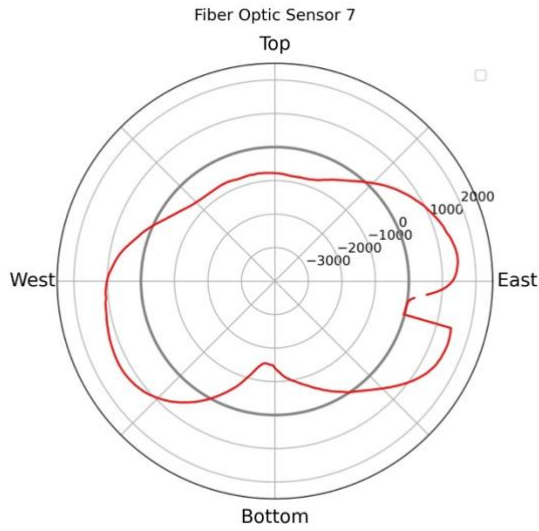
(d) Fiber Optic Sensor F4



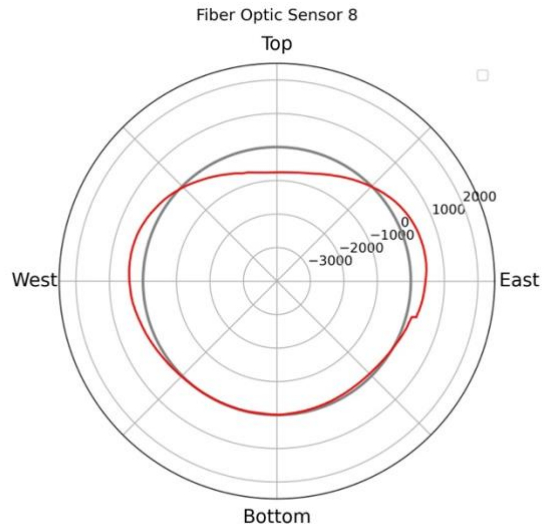
(e) Fiber Optic Sensor F5



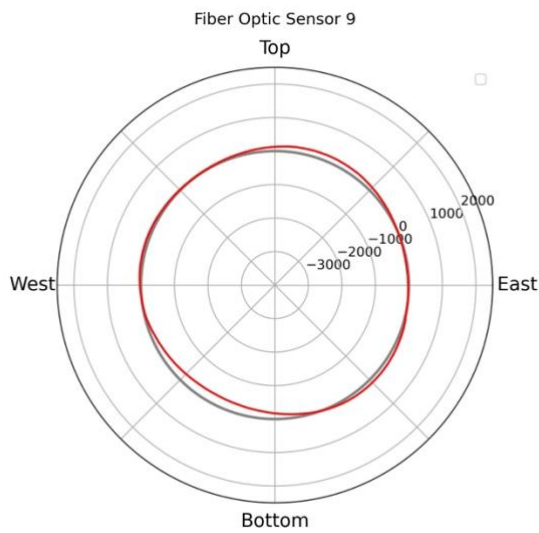
(f) Fiber Optic Sensor F6



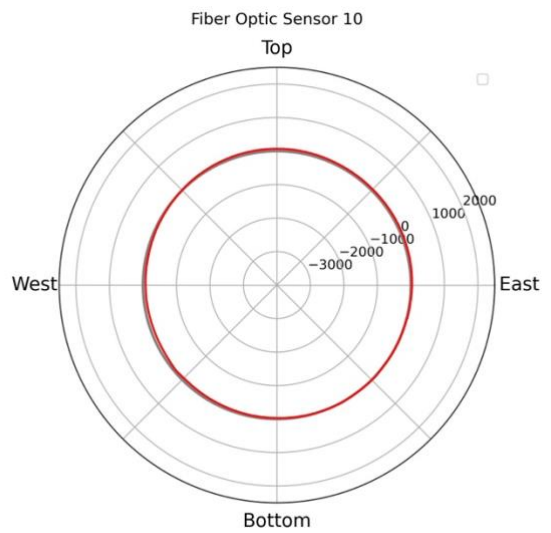
(g) Fiber Optic Sensor F7



(h) Fiber Optic Sensor F8



(i) Fiber Optic Sensor F9



(j) Fiber Optic Sensor F10

Figure B-1 Strain distribution in the circumferential direction